Solar Phys (2009) 259: 49–71
DOI 10.1007/s11207-009-9386-x

What Is the Nature of EUV Waves? First STEREO 3D Observations and Comparison with Theoretical Models

S. Patsourakos · A. Vourlidas · Y.M. Wang · G. Stenborg · A. Thernisien

Received: 10 December 2008 / Accepted: 22 May 2009 / Published online: 3 July 2009

Abstract One of the major discoveries of the Extreme ultraviolet Imaging Telescope (EIT) on SOHO was the intensity enhancements propagating over a large fraction of the solar surface. The physical origin(s) of the so-called EIT waves is still strongly debated with either wave (primarily fast-mode MHD waves) or nonwave (pseudo-wave) interpretations. The difficulty in understanding the nature of EUV waves lies in the limitations of the EIT observations that have been used almost exclusively for their study. They suffer from low cadence and single temperature and viewpoint coverage. These limitations are largely overcome by the SECCHI/EUVI observations onboard the STEREO mission. The EUVI telescopes provide high-cadence, simultaneous multitemperature coverage and two well-separated viewpoints. We present here the first detailed analysis of an EUV wave observed by the EUVI disk imagers on 7 December 2007 when the STEREO spacecraft separation was $\approx 45°$. Both a small flare and a coronal mass ejection (CME) were associated with the wave. We also offer the first comprehensive comparison of the various wave interpretations against the observations. Our major findings are as follows: (1) High-cadence (2.5-minute) 171 Å images showed a strong association between expanding loops and the wave onset and significant

STEREO Science Results at Solar Minimum
Guest Editors: Eric R. Christian, Michael L. Kaiser, Therese A. Kucera, O.C. St. Cyr

Electronic supplementary material The online version of this article (http://dx.doi.org/10.1007/s11207-009-9386-x) contains supplementary material, which is available to authorized users.

S. Patsourakos (✉)
Center for Earth Observing and Space Research, College of Science, George Mason University, Fairfax, VA 22030, USA
e-mail: patsourakos@nrl.navy.mil

A. Vourlidas · Y.M. Wang
Naval Research Laboratory, Space Science Division, Washington, DC 20375, USA

G. Stenborg
Interferometrics, Inc., 13454 Sunrise Valley Drive, Herndon, VA 20171, USA

A. Thernisien
USRA, 10211 Wincopin Circle, Suite 500, Columbia, MD 2104, USA

differences in the wave appearance between the two STEREO viewpoints during its early stages; these differences largely disappeared later; (2) the wave appears at the active region periphery when an abrupt disappearance of the expanding loops occurs within an interval of 2.5 minutes; (3) almost simultaneous images at different temperatures showed that the wave was most visible in the 1 – 2 MK range and almost invisible in chromospheric/transition region temperatures; (4) triangulations of the wave indicate it was rather low lying ($\approx$ 90 Mm above the surface); (5) forward-fitting of the corresponding CME as seen by the COR1 coronagraphs showed that the projection of the best-fit model on the solar surface was inconsistent with the location and size of the co-temporal EUV wave; and (6) simulations of a fast-mode wave were found in good agreement with the overall shape and location of the observed wave. Our findings give significant support for a fast-mode interpretation of EUV waves and indicate that they are probably triggered by the rapid expansion of the loops associated with the CME.

Keywords Flares, dynamics · Corona

1. Introduction

One of the major discoveries of EIT on SOHO (Delaboudinière *et al.*, 1995) was the existence of conspicuous large-scale EUV propagating intensity disturbances. These intensity fronts sometimes have the appearance of an almost circular wave front and are frequently called EIT or EUV waves (*e.g.*, Moses *et al.*, 1997; Thompson *et al.*, 1998, 1999). EUV waves are normally first seen in close proximity to a flaring and erupting active region and they subsequently propagate over a significant fraction of the visible surface before they become too faint to be detected. EIT observations indicate that they travel at speeds of 50 – 400 km s^{-1}. Statistical studies showed that they are mostly associated with coronal mass ejections (CMEs) and not with flares (*e.g.*, Biesecker *et al.*, 2002). There is a tendency for the fastest EUV waves to be associated with similar phenomena in Hα, chromospheric He I, and soft X rays and to produce type II radio bursts (*e.g.*, Moreton, 1960; Athay and Moreton, 1961; Klassen *et al.*, 2000; Kahler and Hudson, 2001; Cliver *et al.*, 2005; Narukage *et al.*, 2002; Hudson *et al.*, 2003; Gilbert *et al.*, 2004; Vršnak *et al.*, 2006). There is an extensive literature on this subject (*e.g.*, Wills-Davey and Thompson, 1999; Delannée, 2000; Klassen *et al.*, 2000; Kahler and Hudson, 2001; Wu *et al.*, 2001; Narukage *et al.*, 2002; Ofman and Thompson, 2002; Gilbert *et al.*, 2004; Zhukov and Auchère, 2004; Podladchikova and Berghmans, 2005; Warmuth and Mann, 2005; Veronig *et al.*, 2006; Vršnak *et al.*, 2006). Reviews on the topic can be found in Chen and Fang (2005), Gopalswamy *et al.* (2006), Pick *et al.* (2006), Schwenn *et al.* (2006), and Warmuth (2007).

Despite the extensive research on these phenomena, significant controversy remains over the physical origin(s) of the EUV waves. One interpretation states that EUV waves are global fast-mode waves triggered by the associated flare or CME (*e.g.*, Thompson *et al.*, 1999; Wang, 2000; Wu *et al.*, 2001; Ofman and Thompson, 2002). The expectation of finding fast-mode waves in the corona was originally considered by Uchida (1968). Fast-mode waves can travel large distances over the solar surface since they can propagate at right angles with respect to the ambient, (radial to a first approximation) magnetic field of the quiet Sun regions, which occupy most of the solar surface, particularly during solar minimum conditions. Moreover, they have a compressive character, which can lead to the intensity enhancement associated with the EUV waves. In what follows we will refer to this interpre-

tation as a *fast-mode wave*. A sufficiently impulsive flare and/or CME can generate a wave or even a shock wave that will then give rise to signatures over an extended range of wavelengths and physical regimes in the solar atmosphere such as EUV waves, Moreton waves (Hα), soft X rays, and type II radio bursts.

Another school of thought states that the EUV waves are not waves at all, but rather they are the signature of the large-scale propagation of the associated CME. We refer to such interpretations as pseudo-waves. One suggestion for a pseudo-wave is the disk projection of the large-scale current shells enveloping the erupting flux rope of the associated CME[1] (Delannée *et al.*, 2008). Using a 3-D MHD flux-rope model Delannée *et al.* (2008) proposed that these currents could be associated with enhanced Ohmic dissipation, leading to coronal heating. This would then result in the enhanced EUV intensities of the wave fronts. It is not known whether this enhanced heating is steady or impulsive in nature. In what follows we will refer to this interpretation as the *current-shell* model for brevity.

A hybrid model, with features from both wave and pseudo-wave models, is the model of Chen *et al.* (Chen *et al.*, 2002; Chen, Fang, and Shibata, 2005; see Chen and Fang, 2005, for a review). This model is based on the eruption of a flux rope and predicts two types of waves: a very fast, super-Alfvénic piston-driven shock straddling the erupting flux rope, which may be identified as the coronal counterpart of a Moreton wave, and a slower pseudo-wave associated with successive opening of the overlying magnetic field induced by the erupting flux rope. The latter type of wave is a pseudo-wave, which Chen *et al.* identify with the EUV waves, and is the result of plasma compression, similar to the conclusion of Delannée and Aulanier (1999), who showed that fast expansion of the magnetic field should compress plasma at the boundaries between expanding stable flux domains, leading to enhanced emission. We will therefore treat the Chen *et al.* model in tandem with the Delannée *et al.* model since both models assert that the EUV waves are formed around the erupting flux rope by either enhanced current shells and/or plasma compression. Note here that Delannée *et al.* (2008) found that the disk projection of the current shells produces more contrast than that from the plasma compression.

Another possibility for a pseudo-wave is successive reconnections between the expanding large-scale CME with small-scale (cool loops) quiet Sun structures (*e.g.*, Attrill *et al.*, 2007a, 2007b; van Driel-Gesztelyi *et al.*, 2008). These reconnection events will give rise to enhanced heating, which will in turn give rise to the bright front intensity. In what follows we will refer to this interpretation as *reconnection fronts*.

Finally, another interesting suggestion regarding the nature of EUV waves is that they represent *MHD solitons* (Wills-Davey, DeForest, and Stenflo, 2007). For solitary waves the wave speed is dependent on the pulse amplitude (a function of density enhancement; Wills-Davey, DeForest, and Stenflo, 2007). As a general trend, the most well defined coronal waves have higher density enhancement and travel faster. More observational signatures from this mechanism need to be worked out to be able to distinguish, for instance, between solitary and nonsolitary waves.

From all this it is clear that understanding the physical origin of EUV waves will supply important constraints on coronal conditions (magnetic field and temperature and density in the corona), for a fast-mode wave interpretation, or on CME initiation and early expansion, for a pseudo-wave interpretation. Part of the problem for conclusively determining the nature of EUV waves stems from the limitations of the EIT observations used almost exclusively

[1] Flux ropes are an integral part of almost all CME models and a large fraction of coronagraphic CME observations provides evidence of such structures.

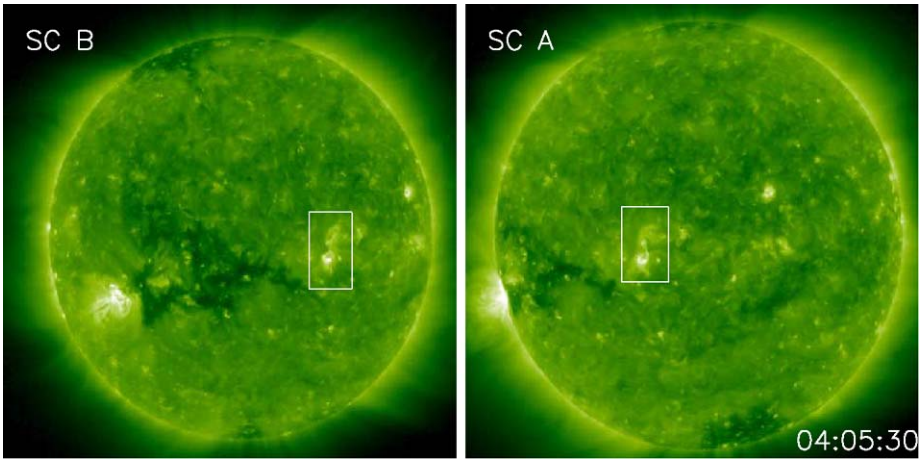

Figure 1 STEREO B (left panel) and A (right panel) full-disk images in the 195 Å channel showing the erupting AR, within the box. The separation between the two spacecraft was $\approx 45°$.

to study these waves: relatively low cadence (12 minutes), one temperature (normally the 195 Å channel) and a single vantage point.

These limitations are largely overcome with the STEREO mission (Kaiser *et al.*, 2008). The Extreme Ultraviolet Imaging Telescope (EUVI; Wülser *et al.*, 2004) of the SECCHI instrument suite (Howard *et al.*, 2008) excels over EIT because of its faster cadence (2.5 minutes or less during campaign periods), simultaneous imaging at different temperature channels, and distinct vantage points allowing a truly 3D view of the Sun. Indeed, previous analyses of EUV waves with high-cadence EUVI data showed that they propagate at higher speeds than previously determined, closer to the magnetoacoustic speed (Long *et al.*, 2008; Veronig, Temmer, and Vršnak, 2008). Additionally, Gopalswamy *et al.* (2009) detected wave reflection from a coronal hole. Finally, Patsourakos and Vourlidas (2007) found evidence of kink-like oscillations of quiet Sun loops in the wake of an EUV wave. MHD simulations showed that EUV waves can induce similar oscillations, at least in the source AR loops (Ofman, 2007). All these findings lend strong support to a wave interpretation.

However, these studies relied on a single viewpoint for their analyses. Here, we present the first stereoscopic study of an EUV wave that occurred on 7 December 2007. Also for the first time, we perform a comprehensive comparison of predictions and/or expectations from each candidate wave interpretation and test them against the STEREO observations. We demonstrate how all the unique advantages of the STEREO observations place new and strong constraints on the nature of EUV waves.

2. Observations and Data Analysis

We analyzed the observations of an EUV wave seen by the two STEREO spacecraft (SC; hereafter A and B) from $\approx$04:30 to 05:15 UT during 7 December 2007. The STEREO spacecraft were significantly separated by $\approx 45°$. The wave was initiated from the small active region 10977, which was close to disk center as viewed by A and toward the east limb as viewed by B (Figure 1). The overall configuration of the corona was rather typical of solar

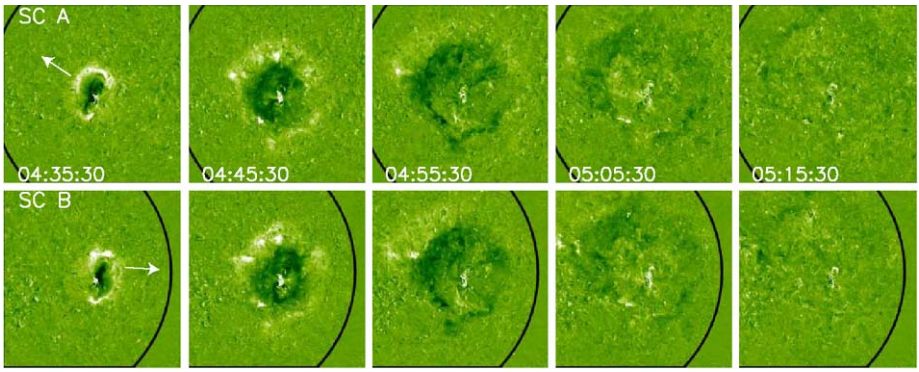

Figure 2 Successive snapshots of the EUV wave in the 195 Å channel for SC A (upper panel) and SC B (lower panel). We display running-ratio images. All images have the same brightness scale. The ratio increases with color from black, to green, to white. The arrows in the first column panels show the oppositely directed loops observed early in the wave event.

minimum conditions: simple active regions, a low-latitude coronal hole, with the rest of the disk dominated by quiet Sun. Close to the time of the wave launch, a small B1.4 class flare started at around 04:35 UT in the same AR and peaked at around 04:41 UT. An associated CME was seen later in coronagraph data. This CME was rather slow, reaching speeds of ≈ 300 km s^{-1} in the coronagraphic fields of view, as determined by *CACTUS* (Robbrecht and Berghmans, 2004), and was not particularly bright.

We focus here on EUV data and total brightness white-light images collected by the EUVI and the COR1 coronagraph (Thompson *et al.*, 2003) on SECCHI, respectively. EUVI takes full-disk images in EUV channels centered around 171, 195, 284, and 304 Å (hereafter referred as 171, 195, 284, and 304). EUVI has ≈ 1.6 arcsec pixels and our observations have a cadence of 2.5, 10, and 20 minutes for 171, 195 – 304, and 284, respectively. COR1 is an internally occulted coronagraph observing from $1.3\,R_\odot$ to $4.0\,R_\odot$. The COR1 pixel size is 15 arcsec and nominal cadence is 15 minutes. The EUVI and COR1 data were processed with the standard *secchi_prep* routine. Note that the EUVI and COR1 image pairs are synchronized; namely, the observations were taken at the same time on the Sun. Therefore, we do not have to worry about the different light travel times from the Sun to the two STEREO spacecraft.

2.1. Multiviewpoint Temporal Behavior

A running-ratio movie of the EUV wave in the 195 channel for both spacecraft can be found online (video1.mov) and representative snapshots from this movie are shown in Figure 2. Each frame corresponds to the ratio of a given 195 image with the previous one. Note here that the cadence of the 195 EUVI data (≈ 10 minutes) is similar to that of EIT (≈ 12 minutes): The basic difference is in the multiview point aspect of the EUVI observations together with the higher sensitivity of EUVI compared to EIT. The latter helps to better observe faint transients like EUV waves. Running-ratio images emphasize changes of the brightness, location, and structure of emitting features between two subsequent images and highlight faint propagating disturbances such as EIT waves. These images correspond to the temporal derivative of the observed intensities. The dark regions do not necessarily represent true dimmings (*e.g.*, Chertok and Grechnev, 2005). We provide a movie of plain

(nondifferenced) 195 Å images (video2.mov), in which each frame has been first processed by a wavelet-based technique (Stenborg, Vourlidas, and Howard, 2008) to increase the image contrast. The propagation of a rather sharp wave front is evident in this movie.

The wave first appears at $\approx$ 04:35 UT at the periphery of the active region, following expanding loop motions, which started around 04:15. After 04:35, the wave starts to expand over the solar surface, becoming progressively more diffuse and faint; after 04:45 it attains a quasi-circular shape and looks similar to data from both spacecraft. The wave seems to avoid the equatorial coronal hole eastward of the source active region. By 05:15 the wave covers a significant part of the visible solar disk, but by this time it is rather diffuse and faint. All these characteristics are pertinent to typical solar minimum EUV waves (*e.g.*, Moses *et al.*, 1997; Thompson *et al.*, 1998).

However, we noticed a peculiarity in the wave propagation early on. Around 04:35 the wave seems to propagate in opposite directions as viewed by the two instruments! It propagates eastward in EUVI-A and westward in EUVI-B (see video1.mov, video2.mov, and Figure 2). At this time the wave is incomplete; it is not forming a full circle.

Higher cadence data are required to resolve this puzzling observation as well as to establish firmer conclusions about the relative timings between different aspects of the event (*e.g.*, flare and loop openings). For this reason, we turn our attention to the 171 images, which were taken at a relatively high cadence of 2.5 minutes. We process them with the a wavelet-based technique to increase the image contrast (Stenborg, Vourlidas, and Howard, 2008). A 171 A and B movie of the area around the source active region is shown in video3.mov. Several snapshots (in running-ratio format to emphasize the motions) from the movie are given in Figure 5. The movie video4.mov shows 171 A and B over a more extended area, covering a significant fraction of the solar disk, to capture the large-scale evolution of the wave. Figure 3 has several snapshots from this movie in running-ratio format.

Several remarks can now be made. First, loops start to slowly rise around 04:11 in A and almost 8 minutes later in B (Figure 3 and video3.mov). They are directed toward the west (east) in B (A), similarly to what is seen in the first column of Figure 2. If we now consider the expanding loops in A indicated by an arrow in the right panel of Figure 3 we note that they are seen more or less face-on. Given the relatively large separation ($\approx 45^\circ$) between A and B these loops should be then seen edge-on in B, as indicated by the arrow in the left panel of Figure 3. Therefore, the oppositely directed early signature of the wave is associated with the expanding motions of the *same* loops observed from the two well-separated viewpoints. Between $\approx$ 04:31:00 and 04:33:30 the expanding loops undergo a sudden jump and can no longer be traced; a wave front starts to develop (Figure 3 and video3.mov). This jump occurs slightly before the start of the associated flare ($\approx$ 04:35). Given that flare onset and impulsive CME acceleration seem to simultaneously occur (*e.g.*, Zhang *et al.*, 2001), it is very possible that the observed loops' jump also marked the start of the impulsive acceleration of the associated CME. The first almost quasi-circular wave front forms around 04:41; the wave also seems to interact with a prominence to the east of the active region at around 04:43 (Figure 4 and video2.mov).

The most important findings of this section – namely, that the wave appeared different (*i.e.*, it exhibited different shapes and direction of propagation) during its early phases from the two distinct vantage points, when loop expansion was clearly observed (*i.e.*, Figures 2, 3, and 5) while later on basically the same quasi-circular pattern was observed – have significant implications. Basically, both pseudo-wave theories expect a quasi-circular wave shape *at all times* (see Delannée *et al.*, 2008; Attrill *et al.*, 2007a), which is clearly in disagreement with our observations. Furthermore, the fact that during later times the wave seems similar on both EUVIs could be a problem for the *current shell* model of Delannée *et al.*

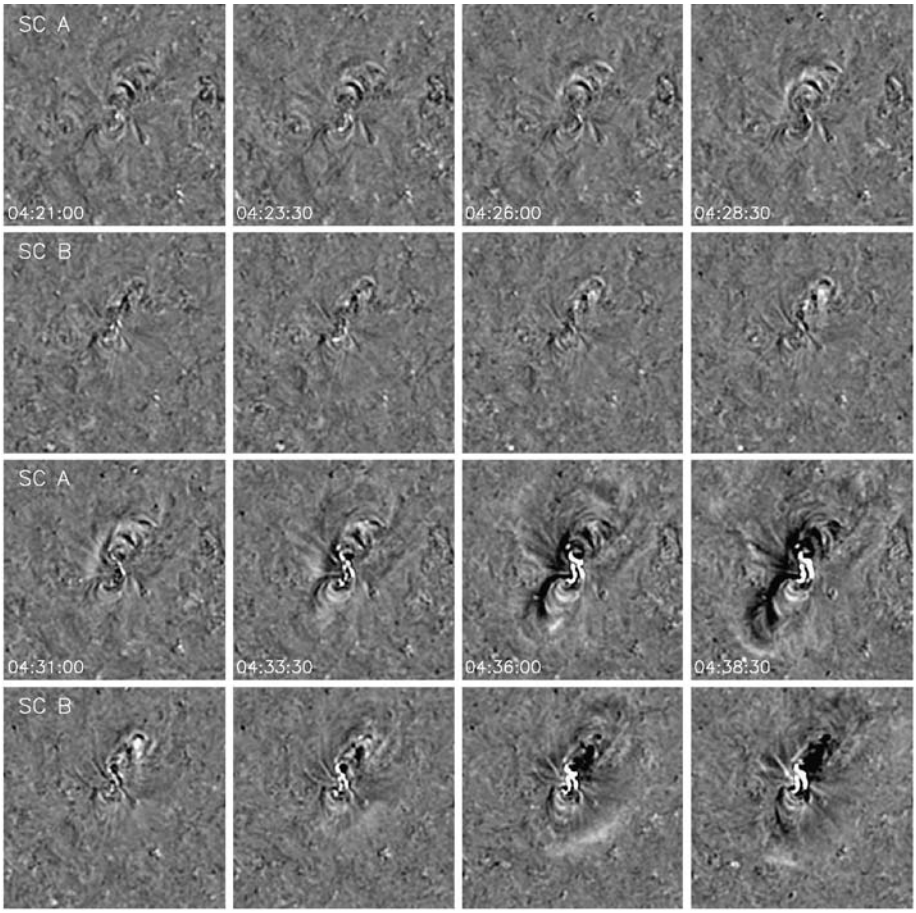

Figure 3 Running-ratio wavelet-enhanced images of the target AR taken in the 171 channels of A and B with a cadence of 2.5 minutes. The same scaling is applied to all images. A four-frame running ratio is taken (*i.e.*, each image is divided by the image taken 10 minutes before). The ratio increases with color from black to white.

(2008), in which the wave is expected to be the disk projection of a very high altitude current shell (280 – 407 Mm), which should appear significantly different from well-separated viewpoints. This is probably not the case for the *reconnection fronts* model of Attrill *et al.* (2007a), in which the wave is assumed to have formed at lower altitudes.

However, a quasi-circular shape is consistent with a wave theory, for which the wave is simply the projection of the 3D wave dome onto the solar surface (*e.g.,* Uchida, 1968; Wang, 2000). To summarize, we find that the *transition* of the wave appearance, from an asymmetric loop expansion early on to a more symmetric and diffuse front, seems to be contrary to the expectations of pseudo-wave theories. These theories invoke symmetric loop expansion at all times, either via "passive" flux-rope eruption or successive reconnections. However, the observed appearance is consistent with a wave driven by an impulsive loop expansion.

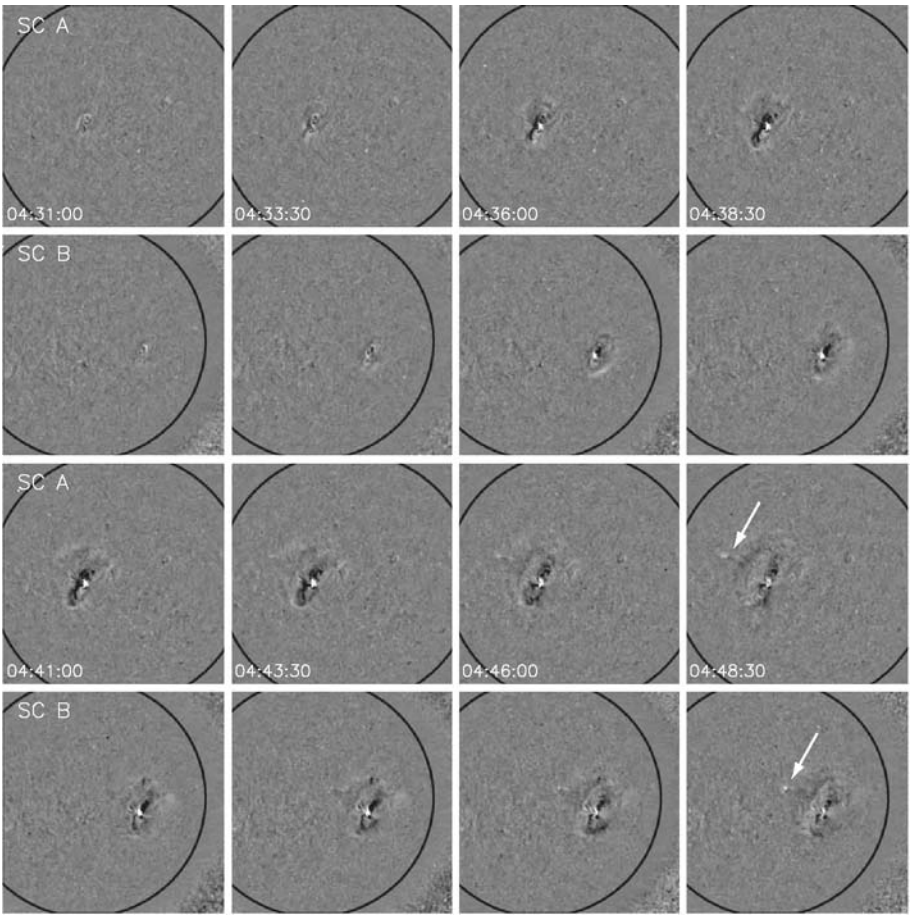

Figure 4 Running-ratio wavelet-enhanced images over an extended area taken in the 171 channels of EUVI-A and EUVI-B with a cadence of 2.5 minutes. A four-frame running ratio is taken (*i.e.*, each image is divided by the image taken 10 minutes before). The same brightness scaling is applied to all images. The ratio increases with color from black to white. The arrows indicate a prominence that was disrupted by the wave.

2.2. Multitemperature Behavior

We now study the wave behavior as a function of temperature. Figure 6 shows almost simultaneous (within a minute) running-ratio images of the wave seen in all bandpasses of EUVI-A, in which the wave was closer to disk center compared to EUVI-B. Note that we used the same 20-minute running-ratio images in all channels, which is the slowest cadence among the EUVI channels. All ratio images have been scaled to the same ratio range and a spatial 3-pixel-wide median filter has been applied to reduce the noise. Azimuthally averaged radial intensity-ratio profiles of the images of Figure 6 are given in Figure 7. They were produced by using a procedure similar to that described by Podladchikova and Berghmans (2005): The image data were first projected onto a spherical polar coordinate system with its center on the flare site, and we then averaged those maps over polar angle to obtain the azimuthally averaged radial intensity-ratio profiles of Figure 7. In this plot the wave front

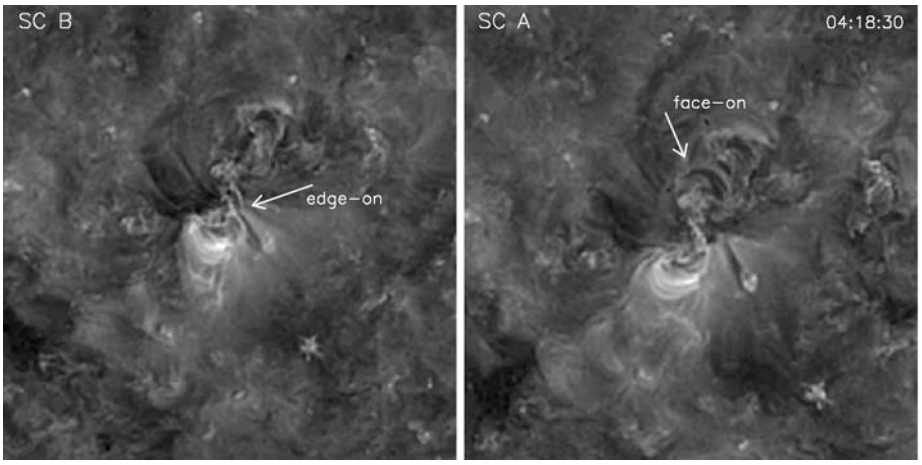

Figure 5 EUVI-A and EUVI-B image pair of wavelet-enhanced 171 images showing the expanding loops associated with the EUV wave onset. The arrows indicate the expanding loops, which are seen edge-on and face-on in B and A, respectively.

is located ahead of a region exhibiting a large-scale minimum of the intensity ratio (radial distances > 250 pixels).

As can be seen from Figures 6 and 7 the wave is visible in the coronal channels of EUVI 171, 195, and 284. It is better defined in 195 while its visibility decreases when going to 284 and 171. In contrast, the wave is barely visible in the mainly chromospheric/transition region 304 channel. The wave in this channel was diffuse and looked similar to what was seen in the 284 channel. The intensity increase associated with the wave takes values in the range of $\approx 5\% - 30\%$.

The wave propagates over quiet Sun regions, where the bulk of the coronal plasma lies in the temperature range of $1-2$ MK, with a peak in the quiet Sun differential emission measure distribution around 1.5 MK (*e.g.* Brosius *et al.*, 1996), a temperature close to the peak of the temperature response function of the 195 channel. The fact that the wave is best seen in this temperature range implies that it represents mostly a density increase without significant plasma heating taking place. Considering also the small intensity increase we conclude that the observed wave represents a small (*i.e.*, linear) density perturbation of the ambient quiet Sun, without any significant plasma heating taking place.

This behavior is consistent with coronal propagation of a fast-mode wave. The wave has a compressive character and when propagating over the quiet Sun corona will compress the ambient plasma, thereby producing intensity increases, which could be the observed wave. Given the much higher densities in the chromosphere/transition region it would be more difficult for a small-amplitude wave to produce significant compression there, which explains the lack of a 304 signature. When the eruption is very fast (greater than several hundred kilometers per second) a shock wave can be produced. This will give rise to significant density and temperature enhancements over a larger temperature range and to sharp wave fronts observed not only in EUV but also in chromospheric emissions Hα and soft X rays (*i.e.*, the "brow" and "S" wave events) as well type II radio bursts (*e.g.*, see the review of Warmuth, 2007).

The observed multitemperature behavior of the wave poses problems to pseudo-wave interpretations. Consider first the *current shell* model of Delannée *et al.* (2008). According

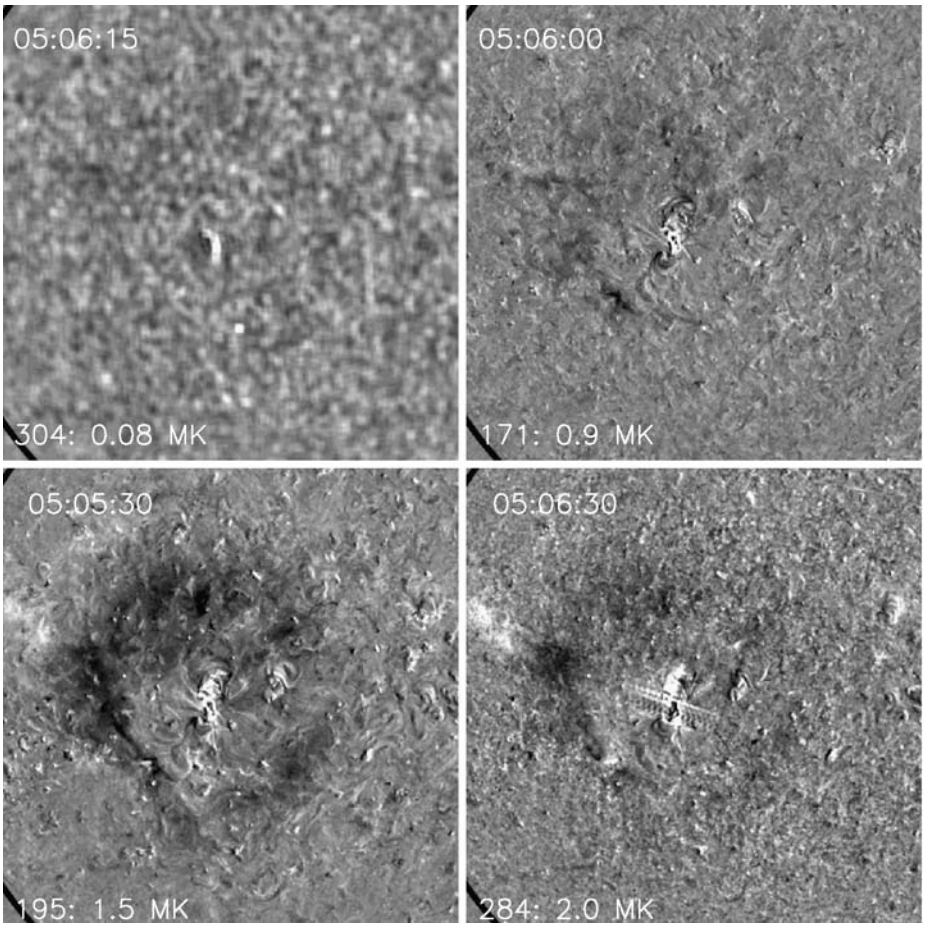

Figure 6 Almost simultaneous snapshots of the EUV wave in the four channels of EUVI-A. The images were taken between 05:05:30 and 05:06:30 UT. The running-ratio images are displayed. All images have the same brightness scaling. The ratio increases with color from black to white. Images have been median-filtered by a three-pixel window to reduce noise in all channels except for 304, where we applied a 15-pixel smoothing to improve the wave visibility.

to this model the wave signature is due to Ohmic heating in large-scale current layers at high altitudes occurring around the erupting flux rope. Note here that our best current theoretical understanding of coronal heating points to rather small-scale currents as a possible heating agent (*e.g.*, Klimchuk, 2006). Moreover, observations show little correlation between large-scale currents and soft X-ray intensities (Fisher *et al.*, 1998).

Note now that the density drops off very rapidly with height in the solar atmosphere (potentially dropping by a factor of $\sim 5-10$ between the base of the corona and 250 Mm; see, for example, Figure 1.20 in the compilation of density measurements of Aschwanden, 2005) and the EUV intensities are proportional to the line-of-sight integral of the density squared. One would then expect that a disk observation in the EUV, such as those of the EUV waves, would be largely dominated by the contribution of the lower (and more dense) layers and not from the higher layers. However, the *current shell* model finds that most

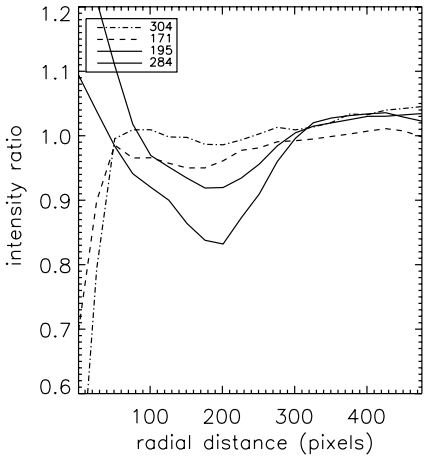

Figure 7 Azimuthally averaged radial intensity-ratio profiles of the images of Figure 6. An EUVI pixel corresponds to ≈ 1.6 arcsec.

of the contribution to the current density should originate from high altitudes (> 250 Mm; Delannée *et al.*, 2008). This discussion implies that the *current shell* model may not lead to any sizeable coronal signal at all.

We now turn our attention to the *reconnection front* model of Attrill *et al.* The observations showed a minimal wave signature in the 304 channel. Note here that the wave did not look substantially better in (plain) 304 images processed by wavelets. This operation has a similar effect on the data as differencing (*i.e.*, enhances subtle features), but it applies to plain images, which takes out some of the ambiguities in the interpretation resulting from taking differences. Moreover, the 304 data of Figure 6 were largely smoothed by a box car of 15 pixels to bring up the wave.

The *reconnection front* model of Attrill *et al.* relies upon small-scale reconnections between the laterally expanding CME and small loops in the surrounding quiet Sun. The energy content in these reconnections would be similar to that associated with the large array of transient phenomena known to occur over the quiet Sun, which are widely believed to be the result of small-scale reconnections (see the review of Parnell, 2002, for example). Therefore, one would expect brightenings of similar magnitude in the frame of the Attrill *et al.* model – which should be easily observable. Note here that the magnitude of these brightenings would be smaller than those occurring in active regions because of the substantially weaker quiet Sun magnetic fields. The typical time scales in the chromosphere/transition region as well as the lifetimes of these transients range from 100 seconds to a few minutes. This means that the relatively low cadence of the 304 data (10 minutes) could cause us to "miss" the moment of maximum emission of some of the brightenings but not all of them. This would give rise to a rather inhomogeneous and more importantly incomplete wave front, which is probably not the case. Higher cadence 304 observations are required to show whether this is really the case.

The footpoints of coronal structures, where the bulk of their transition region/chromospheric emissions come from, represent a very sensitive monitor of coronal conditions. In the case of steady or quasi-steady heating, for example, the transition region emission is proportional to the coronal pressure (*e.g.*, Klimchuk, Patsourakos, and Cargill, 2008, Equation A12). Impulsive heating would give rise to sizeable footpoint emissions, turning them visible in chromospheric/transition region emissions such as 304 (Antiochos *et al.*, 2003; de Pontieu *et al.*, 1999; Hansteen, 1993; Klimchuk, 2006; Klimchuk, Patsourakos, and Cargill, 2008; Martens, Kankelborg, and Berger, 2000; Patsourakos and Klimchuk, 2008;

Spadaro *et al.*, 2006; Winebarger, Warren, and Falconer, 2008). This occurs irrespectively of the spatial location of the heating along individual field lines; thermal conduction and mass flows are very efficient at redistributing any excess heat along the field.

Finally, it is well known observationally that the quiet Sun transition region and chromosphere exhibit stronger variability than the overlying corona (*e.g.*, Berghmans, Clette, and Moses, 1998; Patsourakos and Vial, 2002; Teriaca, Madjarska, and Doyle, 2002). Therefore, if an EUV wave is associated with some sort of impulsive heating, one may expect a significant chromospheric/transition region signature stronger than the coronal one. Our observations show the contrary.

The small impact of the wave in the transition region and the chromosphere may not be a problem for the *current shell* model. This is because the heating in that model occurs on much higher field lines than for the *reconnection front* model. Moreover, as we saw before, footpoint emissions are proportional to the coronal pressure, which in turn is also proportional to the field line length and therefore height for the same temperature (*e.g.*, the scaling-law of Rosner, Tucker, and Vaiana, 1978).

Another potential problem for pseudo-waves concerns their width. Let us first assume a rather low limit for the coronal cooling time of 1000 seconds. Coronal cooling times depend almost linearly on field line length (*e.g.*, Cargill, Mariska, and Antiochos, 1995) and therefore would increase in the expanding field lines associated with a CME and the pseudo-wave. For a typical EUV wave propagation speed of ≈ 300 km s^{-1} one finds that a pseudo-wave should result in a very extended $\approx 3 \times 10^5$ km (or $\approx 0.5 R_\odot$) band of emission in its wake. This is clearly in disagreement with the rather sharply defined wave front observed during the early stages of EUV waves (see, for example, video1.mov and particularly video2.mov with the plain wavelet images). For instance, we estimated a full wave width of ≈ 160 arcsec (*i.e.*, ≈ 110 Mm) for a snapshot of the wave taken at 04:45:30; see Figure 2. This is only 1/7 of $R_\odot$.

We finally comment on the 304 channel emission. Although the passband is dominated by the He II line with a peak temperature of 0.08 MK (upper chromosphere and lower transition region), this passband also contains a contribution from Si XI at 303.32 Å with a peak formation temperature of ≈ 1.6 MK, which is more diffuse than the chromospheric He II emission (*e.g.*, Stenborg, Vourlidas, and Howard, 2008). However, spectrally resolved full-disk CDS observations by Thompson and Brekke (2000) showed that the Si IX contribution in quiet Sun areas is very small (4% of the He II contribution) and diffuse. In our event, the wave signatures in the 304 images are diffuse and faint (similar to the 284 observations), which suggests a likely coronal origin for them. This is problematic for the *reconnection front* interpretation, where, according to the preceding discussion, we should expect low corona/chromospheric signatures *in addition* to the coronal signal.

2.3. Stereoscopic Analysis

Because of the availability of the two SECCHI viewpoints, we are able to estimate the 3D location of the wave. We manually selected several points along a segment of the wave front in an EUVI running-ratio images pair (Figure 8). The segment covered a significant fraction of the wave front so that our measurement can be considered as representative of the structure. We then fitted these points with a parabolic function for each telescope and determined the image (x, y) coordinates of the corresponding vertices. Approximating the wave front with a parabola is a reasonable but by no means unique choice: CME fronts almost universally exhibit concave-outward fronts and wave fronts can be spherically symmetric. Triangulation of the vertex locations using the *scc_triangulate* routine (see Inhester, 2006,

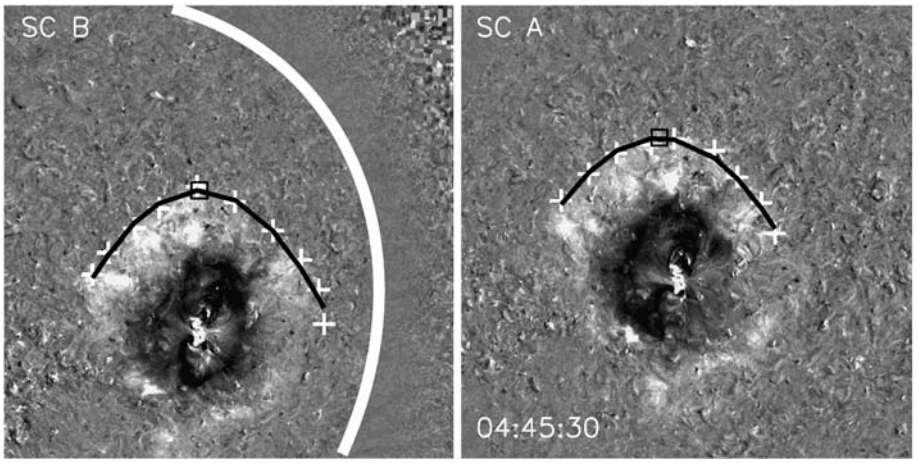

Figure 8 Fitting of segments of the EUV wave front seen in simultaneous EUVI-A and EUVI-B running-ratio images. Both images have the same brightness scaling. Crosses are the points along the wave front selected by point-and-click; the solid black lines are the parabolic fits of the manually selected points. The black boxes are the vertices of the best-fit parabolas.

for the basics of triangulation and stereoscopy) supplied the 3D coordinates (x, y, z) of the vertex of the parabola.

The height h $(=\sqrt{x^2+y^2+z^2} - R_\odot)$ of the wave above the solar surface is about $0.13R_\odot$ or $\approx 90 \pm 7$ Mm (with the error being the standard deviation of the heights determined from ten repetitions of this procedure) and is comparable to the coronal scale height for quiet Sun temperatures (≈ 70 Mm for a temperature of 1.5 MK). This is consistent with fast-mode wave propagation over quiet Sun areas, since the wave perturbs the ambient coronal plasma with its bulk confined within a coronal scale height.

A height of ≈ 90 Mm is probably too small for large-scale current layers around an erupting flux rope of the *current shell* model. Our stereoscopic height observations of the wave of Figure 8 were taken around 30 minutes after loop expansion was first observed and not very far from when the CME first emerged in the COR1 field of view ($1.5R_\odot$), which means that the height of the erupting structure would have been substantially large. Moreover, Delannée *et al.* (2008) expect that the current shells most contributing to the wave should be high-lying ones (> 250 Mm).

Finally, our height measurement is probably too large to be consistent with the *reconnection front* model. The fraction of quiet Sun loops that extend to substantially large heights (> 10 Mm) represents a small fraction of the quiet Sun magnetic flux (10% maximum), with the majority of quiet Sun loops not reaching heights larger than 10 Mm (Close *et al.*, 2004). In the frame of the Attrill *et al.* model, we expect more reconnections to occur between the shorter quiet Sun loops and the expanding flux rope. Also note that since the magnetic field strength decays with height, reconnections employing low-lying quiet Sun loops would be more energetic than those employing larger ones. Therefore, the radiative signal of the wave in the frame of the *reconnection front* model will be dominated by the contribution of the low-lying loops. Larger loops could prevent some of the interactions between the lower loops and the expanding CME but possibly not all of them since the small loops are more numerous.

From this discussion, and given the lack of any predictions on the height of reconnections for the *reconnection front* model, we speculate that the wave height in this scenario

would be that of quiet Sun cool loops, namely, 5 – 10 Mm tall (*e.g.*, Aiouaz and Rast, 2006; Dowdy, Rabin, and Moore, 1986; Feldman, Widing, and Warren, 1999; Close *et al.*, 2004; Patsourakos, Gouttebroze, and Vourlidas, 2007; Peter, 2001; Sánchez Almeida *et al.*, 2007; Tu *et al.*, 2005).

2.4. Pseudo-Wave Modeling

To further test the suggestion that EUV waves could be pseudo-waves directly linked to the CME expansion, we performed forward modeling of the associated CME as seen by COR1.

We used the flux-rope CME model (graduated cylindrical shell; GCS) of Thernisien, Howard, and Vourlidas (2006). GCS is a purely geometrical 3D model aiming to reproduce the large-scale appearance of CMEs in coronagraph data and in particular the CME envelopes; it does not aim to reproduce the fine internal structure of CMEs. It makes no assumption about the physical mechanisms producing the observed CME envelopes. The model consists of a tubular section attached to two cones, which approximate the main body of the flux rope and its legs, respectively. The model is formulated in terms of few adjustable parameters (*i.e.*, location, longitude and latitude of the source region, height of the CME front, *etc.*; see Thernisien, Howard, and Vourlidas, 2006, for details).

The GCS model makes it easy to calculate projections onto the plane of the sky from any viewpoint (*e.g.*, STEREO or SOHO) and compare them with coronagraphic CME observations (COR1 in our case); the free parameters of the model are modified until the best match is found simultaneously in both viewpoints. This requirement makes the model sensitive to changes of its free parameters and therefore results in more accurate CME fits than possible with a single viewpoint (Thernisien, Vourlidas, and Howard, 2009).

We applied the GCS model to an image pair of total brightness COR1 images taken around 05:15 (upper panel of Figure 9). At this time, the wave-associated CME has just emerged above the COR1-B occulter while it was never seen in COR1-A data. Moreover, the EUV wave was still visible on the disk but was rather diffuse (lower panel of Figure 9). To construct Figure 9 we did the following: (1) We found the GCS model best reproducing the associated CME observed by COR1 (upper panel of Figure 9) and (2) we projected the upper (*i.e.*, spherical) section of the model onto the co-temporal EUVI running-ratio images containing the wave (lower panel of Figure 9). Note that step (1) reproduced the large-scale CME seen by COR1-B (top left panel of Figure 9) and indicated that the CME in COR1-A should lie behind the occulting disk (top right panel of Figure 9), as was observed. In step (2) self-similar expansion of the flux-rope-like CME was assumed, as suggested by both observations (Schwenn *et al.*, 2005; Cremades and Bothmer, 2004; Thernisien, Howard, and Vourlidas, 2006; Thernisien, Vourlidas, and Howard, 2009) and models (Török and Kliem, 2005; Attrill *et al.*, 2007a; Delannée *et al.*, 2008).

According to pseudo-wave models, the EUV "waves" correspond to either the disk projection of the CME envelope for the *current shell model* or to the low coronal lateral extent of the CME for the *reconnection fronts model*. Therefore, the procedure of Figure 9 allows us to validate the realism of pseudo-wave models. Note here that our procedure calculates the projection of the upper section of the CME only, and not of its footpoints, which are line-tied to their low corona and presumably correspond to areas of strong dimmings. In principle, the CME envelope will laterally expand either by being "pushed" by the erupting flux rope or by successive reconnections with quiet Sun loops. In any case, the projection of the CME on the low corona – the pseudo-wave – will always follow the CME evolution. Since the GCS model of Figure 9 is constrained by the position and morphology of the CME in the coronagraph data, it accounts for any possible deflections of the CME from

its original propagation direction (*e.g.*, Thernisien, Howard, and Vourlidas, 2006). However, the CME projection disagrees with the actual observed wave in two important aspects: *i*) It is displaced with respect to the wave and *ii*) its projected area is smaller than the wave.

The displacement between the projected CME and the wave is a strong argument toward a freely propagating wave interpretation (with wave and CME propagating independently) and against pseudo-wave models (in which there is a direct link between the CME and the wave). The latter would need to invoke special conditions to account for such displacements. Besides, the often-reported CME deviations (owing to nearby coronal hole boundaries) are based on single-viewpoint observations (LASCO) and therefore may suffer from projection effects. Note here that Delannée *et al.* (2008) show a projection of the current shell from their model on two snapshots of an observed wave, and a good match was found (Figure 11 of Delannée *et al.*, 2008). However, this lacked both the co-temporal snapshot of the associated CME and the multiple lines of sights used in our modeling, thereby not fully constraining the problem. This underlines the importance of multiple viewpoints and of coronagraphs going as close as possible to the solar surface.

The size disparity between CME projection and wave poses another problem for pseudo-wave models, in which by definition they are assumed to be equal. Indeed, if we consider the very rapid decrease of density with height and the strong dependence of EUV intensity on it ($\propto n^2 dl$, with dl the path length along the line of sight) the signal from a disk observation of a CME in the EUV would be dominated by the contribution of its lower sections rather than of its upper sections. Actually, since CMEs expand with height, the disk projection of the CME of Figure 9 largely overestimates its actual size, which makes the comparison between the observed wave and pseudo-wave models even more problematic.

As explained earlier, the disk projection of the GCS model corresponds to the projection of the upper part of CME onto the solar disk, and therefore it does not correspond to the flux-rope footpoints. In Figure 10 we do the inverse. We first find a flux-rope model with a projection on the disk that matches the observed EUV wave simultaneously in A and B. Then we compare its projection on the COR1 images. We believe that this is a good method to test the pseudo-wave model prediction – namely, that the outer CME envelope is the wave. Again, however, we find that the pseudo-wave interpretation cannot account for the observations.

The forward modeling of pseudo-waves of this section is by no means unique, in the sense that different geometries and/or eruption scenarios may be employed. However, as we have explained, the employed geometry (*i.e.*, flux-rope-like and self-similar expansion) find substantial backing in both observations and modeling and therefore represents a reasonable choice. Finally, we note here that if CME and EUV waves had been different facets of the very same phenomenon (*i.e.*, a pseudo-wave), then our fittings of Figures 9 and 10 would have been mutually consistent (*e.g.*, the CMEs of Figures 9 and 10 should have been the same), which is not the case.

For our pseudo-wave modeling we had to use co-temporal images of the wave and the CME. Because of its slow speed, the CME took about 40 minutes after the first appearance of the wave to enter the COR1 field of view. By that time the wave had already traveled over a significant fraction of the solar area and was very diffuse. We have to wait for observations of more impulsive CMEs to perform CME – wave comparisons, with a better defined wave signature.

2.5. Fast-Mode Modeling

Having tested the pseudo-wave interpretation against the observations, we turn to the wave interpretation. We perform a fast-mode wave simulation for the observed EUV wave follow-

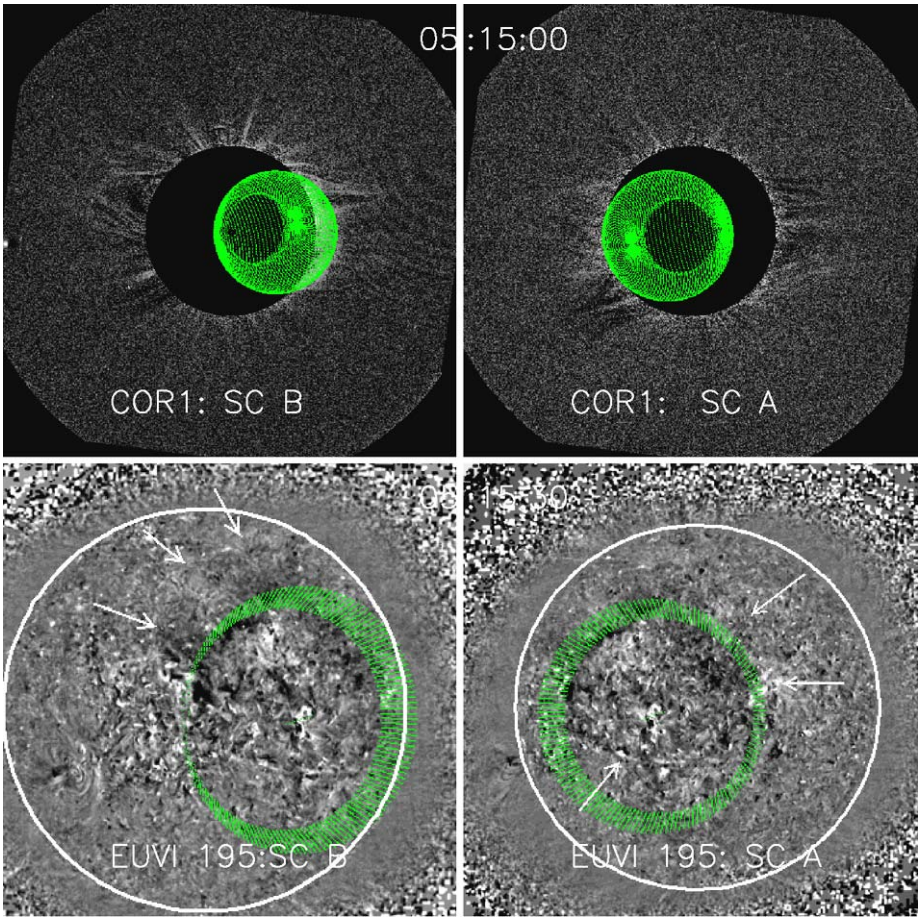

Figure 9 Simultaneous fitting of the CME in COR1-B (upper left) and COR1-A (upper right) with a flux rope model. The best-fit flux rope model is shown in green. COR1 total brightness images are shown in black and white. Pre-CME images were subtracted. Lower panels show the projection (green) of the best-fit flux rope on nearly simultaneous EUVI 195 Å running-ratio images for B (left) and A (right). We consider rather generous extensions for the wave in the north and west direction as indicated by the arrows, which takes care of the uncertainties in defining the wave. The southeast arrow indicates the wave front position in that direction.

ing Wang (2000). First, a potential full source surface extrapolation of the global coronal magnetic field was carried out using MDI synoptic maps centered at the day of our observations. For each traced field line, a hydrostatic isothermal atmosphere at 1.5 MK was then attached following a scaling-law relating density and base magnetic field. These steps supplied the 3D distribution of the fast-mode speed in the corona. Finally, a number of rays were initiated at the periphery of the active region and tracked as a function of time. Essentially the fast-mode wave is diffracted away from regions with high gradients in the fast-mode speed. This happens in active regions (upward wave diffraction) and in coronal holes (diffraction away from the coronal hole). Less diffraction occurs in the quiet Sun, where the fast-mode speed gradients are smoother. Note that the model makes no explicit assumption

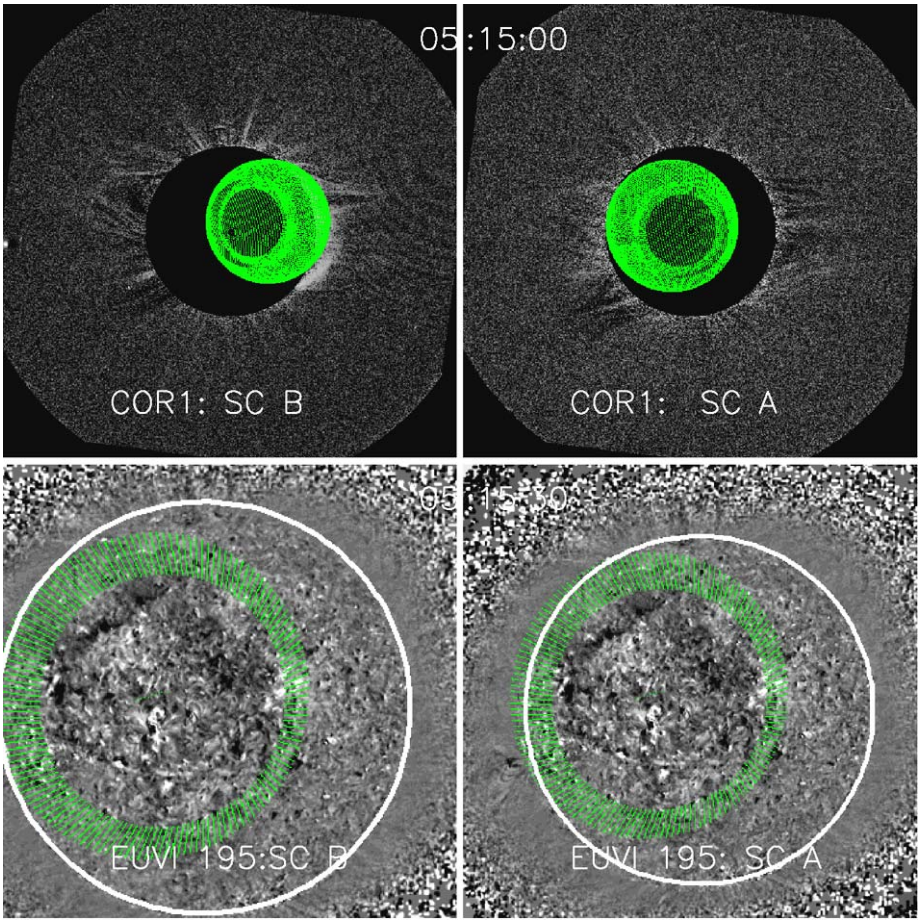

Figure 10 Determining a flux rope CME model with an on-disk projection (green) comparable to the size and location of the observed in an EUVI 195 wave on both B (lower left) and A (lower right panel). Projection (green) of this flux rope model on COR1 total brightness images from B (upper left) and A (upper right) are displayed in black and white. Pre-CME images were first subtracted from the COR1 images. The COR1 and EUVI data were taken almost simultaneously.

about the physical mechanism triggering the wave. For more on the model refer to Wang (2000).

Two snapshots of our simulations are given in Figure 11, where we plot the projection of the wave front (white dotted line) on the solar surface. A viewing point from SOHO has been assumed. The simulated snapshots are separated by 15 minutes, which is also approximately the time separation (12 minutes) between the two running-ratio EIT images (Delaboudinière *et al.*, 1995), which complement Figure 11. We see that the fast-mode simulation essentially manages to track the large-scale appearance of the wave in terms of both size and shape. It follows rather closely the location and shape of the wave between the two successive snapshots and even reproduces some details of the wave, such as the avoidance of the coronal hole.

It is interesting to note that if the wave is launched at the center of the active region, it will expand very rapidly in the radial direction, which is at odds with the observations. The

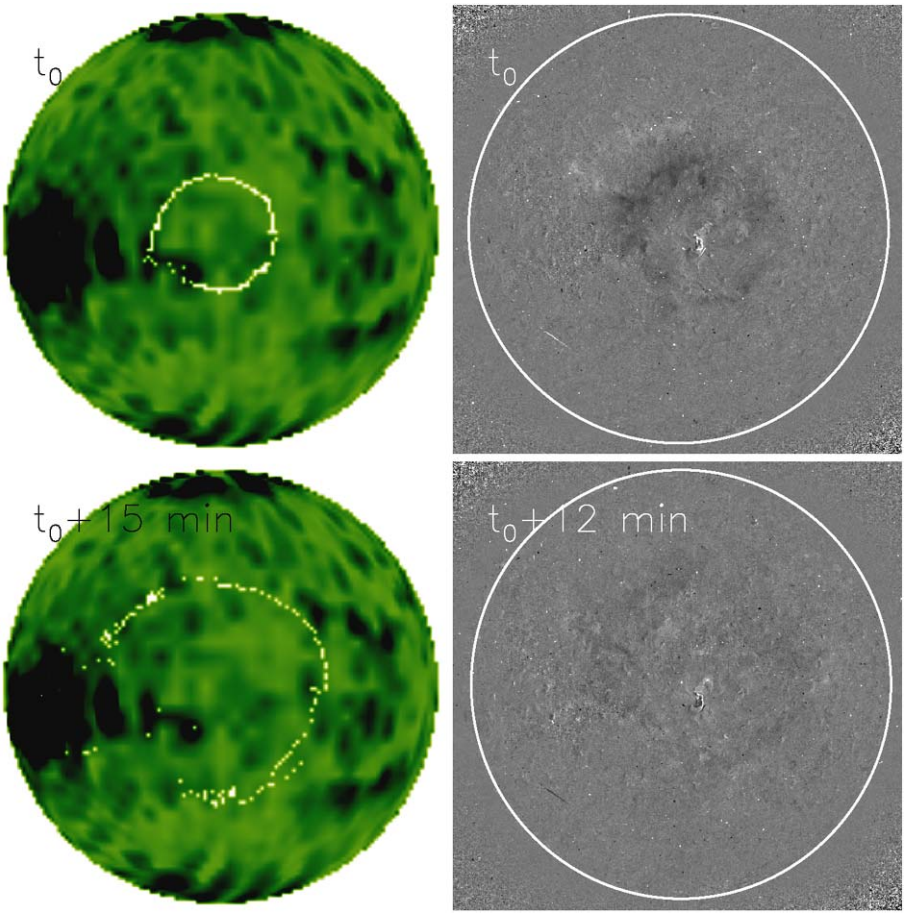

Figure 11 Fast-mode wave simulation of the 7 December 2007 EUV wave (left column) and corresponding EIT running-ratio images (right column). In the left column the location of the wave front projection on the solar surface is indicated by white pixels. It is superimposed on the distribution of the magnetoacoustic speed at the solar surface: black indicates speeds exceeding 500 km s^{-1}; green and white indicate lower speeds. The two snapshots from the simulation are separated by 15 minutes. A SOHO vantage point is assumed. In the right column the two EIT snapshots of the wave are separated by 12 minutes. Both images have the same scaling with ratio increasing with color from black to white.

radial expansion is due to the very rapid decrease of the fast-mode speed with height, which leads to very strong wave diffraction in the upward direction. Instead, the observations in Section 2.1 show that the wave is low lying and appears in the periphery of the active region. This is also a strong argument against the flare as a trigger of the wave since the wave would form at the heart of the active region in that case.

3. Summary and Conclusions

We have performed the first detailed analysis of an EUV wave from two vantage points as observed by the SECCHI disk imagers and coronagraphs. The high cadence and stereoscopic

Table 1 Comparison of the EUVI wave observations to the predictions of various proposed mechanisms to explain EUV waves. The first column gives the physical mechanism, the second column gives the observables, and the third column outlines the observations first and the corresponding model predictions next. TR/chromo = transition region/chromosphere.

Mechanism	Observable	Observations/model predictions
	multiviewpoint appearance	initially asymmetric
		and then ≈ circular
fast-mode wave		≈ circular after wave is set up
current shells		significant differences
reconnection fronts		≈ circular at all times
	multitemperature	(≈ 1 – 2 MK)
fast-mode wave		(≈ 1 – 2 MK)
current shells		weak coronal/TR/chromo
reconnection fronts		TR/chromo
	height	(≈ 90 Mm)
fast-mode wave		coronal scale height (≈ 70 Mm)
current shells		CME height (> 250 Mm)
reconnection fronts		cool loop height (< 10 Mm)
	CME projection	offset and smaller (than the wave)
fast-mode wave		not relevant
current shells		co-spatial and equal
reconnection fronts		co-spatial and equal

observations allowed us for the first time to precisely determine *where* (*i.e.*, in the active region periphery) and *when* (*i.e.*, closely associated with the impulsive acceleration phase of the CME and the start of the associated flare) the first signature of the EUV wave is seen. Our findings place new and tighter constraints on the physics of EUV waves and are summarized as follows:

- High-cadence (2.5-minute) images showed a strong association between expanding loops and the EUV wave onset and significant differences in the wave appearance during early stages as viewed by the two EUV imagers; these differences largely disappear later.
- The wave first appears at the active region periphery when an abrupt jump of the expanding loops occurs within an interval of 2.5 minutes and before the first flare signature.
- The wave is seen more prominently in emissions formed in the ≈ 1 – 2 MK range; little, if anything, is seen in the chromosphere/transition region. The wave represents a rather modest intensity increase of ≈ 5% – 30% over the background.
- Triangulations showed that the wave was low lying with a height of ≈ 70 Mm.
- The on-disk projection of a geometrical flux-rope model of the associated CME did not show good agreement with the observed wave; a disparity of the size and the location of the projection and of the observed wave was found.
- Simulations of a fast-mode wave were found to be in a good agreement with the observed wave.

The comparison of our findings with the expectations of the different proposed mechanisms for EUV waves were discussed and these are summarized in Table 1. We consider that a fast-mode wave is the most probable interpretation. Pseudo-wave theories run into

significant trouble when trying to reconcile several important elements of the observations: an asymmetric-to-symmetric transition in the wave appearance as seen from the two SC, a rather poor chromospheric/transition region signature (inconsistent at least with the *reconnection front* model), probably too small a wave height for the *current shell* model and too large for the *reconnection front* model, and a missmatching CME on-disk projection with respect to the observed wave. However, a fast-mode wave interpretation is consistent with all observations.

We wish to iterate here that by EUV waves we are exclusively referring to large-scale propagating intensity enhancements, which reach significant distances from the source region, especially during periods of solar minimum when the coronal landscape is rather simple. We do not exclude the possibility that other propagating intensity fronts that follow closely the expanding dimmings could indeed be pseudo-waves. However, these dimmings would normally never reach the rather global scales of the EUV waves we are considering here. Statistical studies of EUV dimming showed an average width of only $\approx 36^\circ$ (Reinard and Biesecker, 2008). We think that models such as the hybrid model of Chen *et al.* may be able to explain both the dimming and the "true" wave. Further MHD simulations mapping the parameter space of different CME – wave-dimming scenarios are required.

We can now draw the following picture about the observed EUV wave. Coronal loops start to slowly expand (*e.g.*, Figure 3 and video3.mov). This happens clearly before the onset of the flare. The angular separation of our observations was large enough ($\approx 45^\circ$) to allow us to observe the *same* loops from strikingly different perspectives early on in the event (edge-on and face on; first column of Figure 2 and Figure 5). Just before the start of the associated flare, the loops abruptly disappear and can no longer be traced; a well-defined wave front forms at the periphery of the active region. This front could be generated by a large-scale disturbance induced by either the impulsive CME acceleration or the associated flare. The latter possibility can be rather safely excluded for the following reasons: (1) The associated flare was weak and (2) we found in Section 2.5 that launching the wave in the active region core, as expected from a flare-associated blast wave, would not lead to wave fronts consistent with the observations. It is possible that the catastrophic energy release that apparently destroys the ascending loops within 2.5 minutes is also responsible for the launch of the wave, which starts to propagate freely. A freely propagating wave is consistent with the fact that the wave becomes more diffuse as it propagates farther from the active region (*e.g.*, Parker, 1961; Hundhausen, 1985; Warmuth, 2007).

Before closing we note that clearly more work from both observational and theoretical approaches is required. First, although the analyzed event could be considered as a "typical" solar minimum EUV wave, our study needs to be extended to larger sets of EUV wave events seen by STEREO. More emphasis should be given to higher cadence wave observations in the 195 Å channel, in which waves are best visible, to obtain a larger number of useable measurements per event. Moreover, higher cadence is needed also in the 304 Å channel to search for evidence of transient brightenings that could be associated with reconnection fronts. Combination of stereoscopic wave observations by STEREO with the ultra-high-cadence EUV observations from SDO will certainly help in that direction.

Finally, we note that the theories of EUV waves have reached various degrees of sophistication. However, none of these theories are yet at a level to construct synthetic EUV images out of the particular physical mechanism to allow direct comparison with the observations. For this reason, we relied in this study upon morphological concepts such as wave fronts, CME projections, and geometrical shapes, which have led us to physical insights but are not sufficiently quantitative, at least to our satisfaction. We welcome the recent development of the full-Sun MHD models of Linker *et al.* (2008), which treat in a self-consistent manner both the CME eruption (*i.e.*, the wave driver) and plasma thermodynamics (*i.e.*, what it

ultimately required for calculating realistic EUV intensities). Their simulated EUV images showed the appearance of propagating intensity fronts similar to typical EUV waves. The analysis of these fronts showed that they could be identified as a fast-mode wave.

Acknowledgements The SECCHI data used here were produced by an international consortium of the Naval Research Laboratory (USA), Lockheed Martin Solar and Astrophysics Lab (USA), NASA Goddard Space Flight Center (USA), Rutherford Appleton Laboratory (UK), University of Birmingham (UK), Max-Planck-Institut for Solar System Research (Germany), Centre Spatiale de Liège (Belgium), Institut d'Optique Théorique et Appliqueé (France), and Institut d'Astrophysique Spatiale (France). We sincerely thank the referee for many useful comments that led to a significant improvement of the manuscript. We thank G. Attrill, L. van Driel-Gesztelyi, E. Robbrecht, H. Hudson, S. Plunkett, J. Linker, S. Krucker, and M. Pick for useful discussions.

References

Aiouaz, T., Rast, M.P.: 2006, *Astrophys. J.* **647**, L183.
Antiochos, S.K., Karpen, J.T., DeLuca, E.E., Golub, L., Hamilton, P.: 2003, *Astrophys. J.* **590**, 547.
Aschwanden, M.J.: 2005, *Physics of the Solar Corona. An Introduction with Problems and Solutions*, Praxis Publ. Ltd., Chichester; Springer, New York, ISBN 3-540-30765-6.
Athay, R.G., Moreton, G.E.: 1961, *Astrophys. J.* **133**, 935.
Attrill, G.D.R., Harra, L.K., van Driel-Gesztelyi, L., Démoulin, P., Wülser, J.-P.: 2007a, *Astron. Nachr.* **328**, 760.
Attrill, G.D.R., Harra, L.K., van Driel-Gesztelyi, L., Démoulin, P.: 2007b, *Astrophys. J.* **656**, L101.
Berghmans, D., Clette, F., Moses, D.: 1998, *Astron. Astrophys.* **336**, 1039.
Biesecker, D.A., Myers, D.C., Thompson, B.J., Hammer, D.M., Vourlidas, A.: 2002, *Astrophys. J.* **569**, 1009.
Brosius, J.W., Davila, J.M., Thomas, R.J., Monsignori-Fossi, B.C.: 1996, *Astrophys. J. Suppl.* **106**, 143.
Cargill, P.J., Mariska, J.T., Antiochos, S.K.: 1995, *Astrophys. J.* **439**, 1034.
Chen, P.F., Fang, C.: 2005, In: Dere, K.P., Wang, J., Yan, Y. (eds.) *Coronal and Stellar Mass Ejections, Proc. IAU Symp.* **226**, 55.
Chen, P.F., Fang, C., Shibata, K.: 2005, *Astrophys. J.* **622**, 1202.
Chen, P.F., Wu, S.T., Shibata, K., Fang, C.: 2002, *Astrophys. J.* **572**, L99.
Chertok, I.M., Grechnev, V.V.: 2005, *Solar Phys.* **229**, 95.
Cliver, E.W., Laurenza, M., Storini, M., Thompson, B.J.: 2005, *Astrophys. J.* **631**, 604.
Close, R.M., Parnell, C.E., Longcope, D.W., Priest, E.R.: 2004, *Astrophys. J.* **612**, L81.
Cremades, H., Bothmer, V.: 2004, *Astron. Astrophys.* **422**, 307.
Delaboudinière, J.-P., Artzner, G.E., Brunaud, J., Gabriel, A.H., Hochedez, J.F., Millier, F., Song, X.Y., Au, B., Dere, K.P., Howard, R.A., Kreplin, R., Michels, D.J., Moses, J.D., Defise, J.M., Jamar, C., Rochus, P., Chauvineau, J.P., Marioge, J.P., Catura, R.C., Lemen, J.R., Shing, L., Stern, R.A., Gurman, J.B., Neupert, W.M., Maucherat, A., Clette, F., Cugnon, P., van Dessel, E.L.: 1995, *Solar Phys.* **162**, 291.
Delannée, C.: 2000, *Astrophys. J.* **545**, 512.
Delannée, C., Aulanier, G.: 1999, *Solar Phys.* **190**, 107.
Delannée, C., Török, T., Aulanier, G., Hochedez, J.-F.: 2008, *Solar Phys.* **247**, 123.
de Pontieu, B., Berger, T.E., Schrijver, C.J., Title, A.M.: 1999, *Solar Phys.* **190**, 419.
Dowdy, J.F. Jr., Rabin, D., Moore, R.L.: 1986, *Solar Phys.* **105**, 35.
Feldman, U., Widing, K.G., Warren, H.P.: 1999, *Astrophys. J.* **522**, 1133.
Fisher, G.H., Longcope, D.W., Metcalf, T.R., Pevtsov, A.A.: 1998, *Astrophys. J.* **508**, 885.
Gilbert, H.R., Holzer, T.E., Thompson, B.J., Burkepile, J.T.: 2004, *Astrophys. J.* **607**, 540.
Gopalswamy, N., Mikić, Z., Maia, D., Alexander, D., Cremades, H., Kaufmann, P., Tripathi, D., Wang, Y.-M.: 2006, *Space Sci. Rev.* **123**, 303.
Gopalswamy, N., Yashiro, S., Temmer, M., Davila, J., Thompson, W.T., Jones, S., McAteer, R.T.J., Wuelser, J.-P., Freeland, S., Howard, R.A.: 2009, *Astrophys. J.* **691**, L123.
Hansteen, V.: 1993, *Astrophys. J.* **402**, 741.
Howard, R., Moses, J.D., Vourlidas, A., Newmark, J.S., Socker, D.G., Plunkett, S.P., Korendyke, C.M., Cook, J.W., Hurley, A., Davila, J.M., *et al.*: 2008, *Space Sci. Rev.* **136**, 37.
Hudson, H.S., Khan, J.I., Lemen, J.R., Nitta, N.V., Uchida, Y.: 2003, *Solar Phys.* **212**, 121.
Hundhausen, A.J.: 1985, In: Stone, R.G., Tsurutani, B.T. (eds.) *Collisionless Shocks in the Heliosphere: A Tutorial Review, Geophys. Monogr. Ser.* **34**, AGU, Washington, 37.

Inhester, B.: 2006, Preprint. astr-ph/0612649.
Kahler, S.W., Hudson, H.S.: 2001, *J. Geophys. Res.* **106**, 29239.
Kaiser, M.L., Kucera, T.A., Davila, J.M., St. Cyr, O.C., Guhathakurta, M., Christian, E.: 2008, *Space Sci. Rev.* **136**, 5.
Klassen, A., Aurass, H., Mann, G., Thompson, B.J.: 2000, *Astron. Astrophys. Suppl. Ser.* **141**, 357.
Klimchuk, J.A.: 2006, *Solar Phys.* **234**, 41.
Klimchuk, J.A., Patsourakos, S., Cargill, P.J.: 2008, *Astrophys. J.* **682**, 1351.
Linker, J.A., Lionello, R., Mikic, Z., Titov, V., Riley, P.: 2008, AGU Spring Meeting Abstracts, SP31D-05.
Long, D.M., Gallagher, P.T., McAteer, R.T.J., Bloomfield, D.S.: 2008, *Astrophys. J.* **680**, L81.
Martens, P.C.H., Kankelborg, C.C., Berger, T.E.: 2000, *Astrophys. J.* **537**, 471.
Moreton, G.E.: 1960, *Astron. J.* **65**, 494.
Moses, D., Clette, F., Delaboudinière, J.-P., Artzner, G.E., Bougnet, M., Brunaud, J., Carabetian, C., Gabriel, A.H., Hochedez, J.F., Millier, F., *et al.*: 1997, *Solar Phys.* **175**, 571.
Narukage, N., Hudson, H.S., Morimoto, T., Akiyama, S., Kitai, R., Kurokawa, H., Shibata, K.: 2002, *Astrophys. J.* **572**, L109.
Ofman, L., Thompson, B.J.: 2002, *Astrophys. J.* **574**, 440.
Ofman, L.: 2007, *Astrophys. J.* **655**, 1134.
Parker, E.N.: 1961, *Astrophys. J.* **133**, 1014.
Parnell, C.E.: 2002, In: *SOLMAG 2002. Proceedings of the Magnetic Coupling of the Solar Atmosphere Euroconference* **505**, 231.
Patsourakos, S., Klimchuk, J.A.: 2008, *Astrophys. J.* **689**, 1406.
Patsourakos, S., Vial, J.-C.: 2002, *Astron. Astrophys.* **385**, 1073.
Patsourakos, S., Vourlidas, A.: 2007, *AGU Fall Meeting Abstracts*, A779.
Patsourakos, S., Gouttebroze, P., Vourlidas, A.: 2007, *Astrophys. J.* **664**, 1214.
Peter, H.: 2001, *Astron. Astrophys.* **374**, 1108.
Pick, M., Forbes, T.G., Mann, G., Cane, H.V., Chen, J., Ciaravella, A., Cremades, H., Howard, R.A., Hudson, H.S., Klassen, A., Klein, K.L., Lee, M.A., Linker, J.A., Maia, D., Mikic, Z., Raymond, J.C., Reiner, M.J., Simnett, G.M., Srivastava, N., Tripathi, D., Vainio, R., Vourlidas, A., Zhang, J., Zurbuchen, T.H., Sheeley, N.R., Marqué, C.: 2006, *Space Sci. Rev.* **123**, 341.
Podladchikova, O., Berghmans, D.: 2005, *Solar Phys.* **228**, 265.
Robbrecht, E., Berghmans, D.: 2004, *Astron. Astrophys.* **425**, 1097.
Rosner, R., Tucker, W.H., Vaiana, G.S.: 1978, *Astrophys. J.* **220**, 643.
Reinard, A.A., Biesecker, D.A.: 2008, *Astrophys. J.* **674**, 576.
Sánchez Almeida, J., Teriaca, L., Sütterlin, P., Spadaro, D., Schühle, U., Rutten, R.J.: 2007, *Astron. Astrophys.* **475**, 1101.
Schwenn, R., dal Lago, A., Huttunen, E., Gonzalez, W.D.: 2005, *Ann. Geophys.* **23**, 1033.
Schwenn, R., Raymond, J.C., Alexander, D., Ciaravella, A., Gopalswamy, N., Howard, R., Hudson, H., Kaufmann, P., Klassen, A., Maia, D., Munoz-Martinez, G., Pick, M., Reiner, M., Srivastava, N., Tripathi, D., Vourlidas, A., Wang, Y.-M., Zhang, J.: 2006, *Space Sci. Rev.* **123**, 127.
Spadaro, D., Lanza, A.F., Karpen, J.T., Antiochos, S.K.: 2006, *Astrophys. J.* **642**, 579.
Stenborg, G., Vourlidas, A., Howard, R.A.: 2008, *Astrophys. J.* **674**, 1201.
Teriaca, L., Madjarska, M.S., Doyle, J.G.: 2002, *Astron. Astrophys.* **392**, 309.
Thernisien, A.F.R., Howard, R.A., Vourlidas, A.: 2006, *Astrophys. J.* **652**, 763.
Thernisien, A.F.R., Vourlidas, A., Howard, R.A.: 2009, *Solar Phys.* **256**, 111.
Thompson, B.J., Plunkett, S.P., Gurman, J.B., Newmark, J.S., St. Cyr, O.C., Michels, D.J.: 1998, *Geophys. Res. Lett.* **25**, 2465.
Thompson, B.J., Gurman, J.B., Neupert, W.M., Newmark, J.S., Delaboudinière, J.-P., St. Cyr, O.C., Stezelberger, S., Dere, K.P., Howard, R.A., Michels, D.J.: 1999, *Astrophys. J.* **517**, L151.
Thompson, W.T., Brekke, P.: 2000, *Solar Phys.* **195**, 45.
Thompson, W.T., Davila, J.M., Fisher, R.R., Orwig, L.E., Mentzell, J.E., Hetherington, S.E., Derro, R.J., Federline, R.E., Clark, D.C., Chen, P.T.C., *et al.*: 2003, In: *Innovative Telescopes and Instrumentation for Solar Astrophysics*, *SPIE* **4853**, 1.
Török, T., Kliem, B.: 2005, *Astrophys. J.* **630**, L97.
Tu, C.-Y., Zhou, C., Marsch, E., Wilhelm, K., Zhao, L., Xia, L.-D., Wang, J.-X.: 2005, *Astrophys. J.* **624**, L133.
Uchida, Y.: 1968, *Solar Phys.* **4**, 30.
van Driel-Gesztelyi, L., Attrill, G.D.R., Démoulin, P., Mandrini, C.H., Harra, L.K.: 2008, *Ann. Geophys.* **26**, 3077.
Veronig, A.M., Temmer, M., Vršnak, B., Thalmann, J.K.: 2006, *Astrophys. J.* **647**, 1466.
Veronig, A.M., Temmer, M., Vršnak, B.: 2008, *Astrophys. J.* **681**, L113.

Vršnak, B., Warmuth, A., Temmer, M., Veronig, A., Magdalenić, J., Hillaris, A., Karlický, M.: 2006, *Astron. Astrophys.* **448**, 739.
Wang, Y.-M.: 2000, *Astrophys. J.* **543**, L89.
Warmuth, A.: 2007, In: *Lecture Notes in Physics* **725**, Springer, Berlin, 107.
Warmuth, A., Mann, G.: 2005, *Astron. Astrophys.* **435**, 1123.
Wills-Davey, M.J., Thompson, B.J.: 1999, *Solar Phys.* **190**, 467.
Wills-Davey, M.J., DeForest, C.E., Stenflo, J.O.: 2007, *Astrophys. J.* **664**, 556.
Winebarger, A.R., Warren, H.P., Falconer, D.A.: 2008, *Astrophys. J.* **676**, 672.
Wu, S.T., Zheng, H., Wang, S., Thompson, B.J., Plunkett, S.P., Zhao, X.P., Dryer, M.: 2001, *J. Geophys. Res.* **106**, 25089.
Wülser, J.-P., Lemen, J.R., Tarbell, T.D., Wolfson, C.J., Cannon, J.C., Carpenter, B.A., Duncan, D.W., Gradwohl, G.S., Meyer, S.B., Moore, A.S.: 2004, *Proc. SPIE* **5171**, 111.
Zhang, J., Dere, K.P., Howard, R.A., Kundu, M.R., White, S.M.: 2001, *Astrophys. J.* **559**, 452.
Zhukov, A.N., Auchère, F.: 2004, *Astron. Astrophys.* **427**, 705.